Efficient Separation between Projected Patterns
for Multiple Projector 3D People Scanning

Tomislav Petković, Tomislav Pribanić and Matea Đonlić
University of Zagreb Faculty of Electrical Engineering and Computing
Unska 3, HR-10000 Zagreb, Croatia
{tomislav.petkovic.jr, tomislav.pribanic, matea.donlic}@fer.hr

Peter Sturm
INRIA Grenoble Rhône-Alpes
Inovallée, 655 Avenue de l'Europe, Montbonnot, 38334 Saint Ismier Cedex, France
peter.sturm@inria.fr

Abstract

Structured light 3D surface scanners are usually comprised of one projector and of one camera which provide a limited view of the object's surface. Multiple projectors and cameras must be used to reconstruct the whole surface profile. Using multiple projectors in structured light profilometry is a challenging problem due to inter-projector interferences which make pattern separation difficult. We propose the use of sinusoidal fringe patterns where each projector has its own specifically chosen set of temporal phase shifts which together comprise a DFT_{2P+1} basis, where P is the number of projectors. Such a choice enables simple and efficient separation between projected patterns. The proposed method does not impose a limit on the number of projectors used and does not impose a limit on the projector placement. We demonstrate the applicability of the proposed method on three projectors and six cameras structured light system for human body scanning.

1. Introduction

Structured light (SL) 3D surface scanning using sinusoidal patterns, the *fringe projection profilometry* (FPP), is one of the most robust and well accepted techniques in practical applications including (but not limited to) human body scanning, digital model generation, reverse engineering, rapid prototyping, and quality control [7]. In FPP a projector projects a sinusoidal fringe pattern onto a object which is then recorded by a camera. The phase of the deformed fringe pattern observed by the camera encodes all information required to reconstruct the surface profile.

In many applications of FPP a complete object's surface profile is required. Obtaining a complete surface profile is impossible using only one projector and only one camera due to occlusions and limited fields of view. While adding a camera to a FPP system is simple, adding a projector to increase the illuminated area is a challenging problem due to interference between projected patterns. Indeed, almost all of SL patterns described in the literature [21, 22, 1] are designed for a single projector. Considering that the only option for using the existing SL patterns in a multi-projector SL system is to use projectors in turns which eliminates any interference [5].

There are currently only several multi-projector FPP systems described in the literature which employ simultaneous pattern projection. Servin et al. [24, 25] describe a multi-projector single-camera system which relies on a very precise spatial placement of projectors (so called co-phased profilometry), and therefore has limited general applicability. Woolford and Burnett [29] describe a more general two-projector multi-camera system which uses spatial fringe multiplexing where spatial orientations of fringe patterns vary between projectors: one projector uses vertical and another horizontal fringes. Such spatial fringe multiplexing is commonly used in single-projector FPP systems [31, 27], however, in multi-projector FPP systems it places undesirable constraints on spatial projector placement and is not easily extendable to an arbitrary number of projectors. Interestingly, multi-projector FPP systems which use an acquisition strategy where projectors are employed sequentially are also rarely described [26, 5]

Non FPP-based multi-projector multi-camera systems are also uncommon in the literature. Sagawa et al. [20, 19] describe a multi-projector system which uses line patterns with different spatial line orientations. Similar to spatial

multiplexing in FPP systems [29, 31] using different spatial orientations places undesirable constraints on spatial projector placement. Yan et al. [30] describe a theoretical multi-projector system which combines De Bruijn color sequences and random dot patterns; unfortunately, their work only provides simulated results making practical applicability questionable.

We propose a novel multi-projector multi-camera structured light surface scanning system which uses gray-level sinusoidal fringe patterns where each projector has its own carefully chosen set of temporal phase shifts. The idea of separating mixed sinusoids from a sufficient number of observations was previously applied to single projector FPP systems [16, 9, 8] only. In our approach for a scanner using P projectors we select temporal phase shifts to comprise a discrete Fourier transform in $2P + 1$ points (DFT_{2P+1}) which enables simple and efficient decoupling of projected fringes. Compared to existing multi-projector multi-camera FPP systems the proposed method does not impose a limit on the number of projectors used and does not impose constraints on the projector placement. To the best of our knowledge there is currently no multi-projector multi-camera FPP system described in the literature which does not impose constraints on projector placement.

This paper is organized as follows: In Section 2 we present the proposed method. In Section 3 we compare the proposed method to classical sequential employment. Results and discussion are presented in Section 3. We conclude in Section 5.

2. The Proposed Method

Before presenting the proposed method we give a brief review of a classical one-projector temporal phase shifting strategy [2, 11]. We then extend this first to the two-projectors case in Section 2.2 and then to the arbitrary number of projectors in Section 2.3.

2.1. Classical Temporal Phase Shifting

Classical approaches to temporal phase shifting use one projector only. The projector projects a set of N phase-shifted gray-level sinusoidal fringes which are observed by one or more cameras sequentially in time. Each of N projected fringes has a different temporal phase shift $\varphi[n]$ given by

$$\varphi[n] = 2\pi n/N, \quad n = 0, \dots, N-1, \quad (1)$$

where n is a frame number (time-step). The intensity of the nth fringe in projector's coordinate system $(x_{\mathrm{PRJ}}, y_{\mathrm{PRJ}})$ is:

$$I_{\mathrm{PRJ}}(x_{\mathrm{PRJ}}, y_{\mathrm{PRJ}}) = I_0\big(1 + \cos(\omega x_{\mathrm{PRJ}} + \varphi[n])\big)/2, \quad (2)$$

where I_0 is projector's intensity and where ω is spatial frequency. The intensity of the nth fringe observed by

the camera and expressed in camera's coordinate system $(x_{\mathrm{CAM}}, y_{\mathrm{CAM}})$ is:

$$I_{\mathrm{CAM}}(x_{\mathrm{CAM}}, y_{\mathrm{CAM}}) = I_{\mathrm{AMB}} + hI_{\mathrm{PRJ}}, \quad (3)$$

where I_{AMB} is a constant ambient illumination and where h, $0 \le h < 1$, models pixel-dependent channel loss. Combining Eqs. (2) and (3) yields:

$$I_{\mathrm{CAM}}(x_{\mathrm{CAM}}, y_{\mathrm{CAM}}) = a + b\cos(\omega x_{\mathrm{PRJ}} + \varphi[n]), \quad (4)$$

where $a = I_{\mathrm{AMB}} + \frac{1}{2}hI_0$ is a time-invariant component comprised of both ambient and projector illumination and where $b = \frac{1}{2}hI_0$ is the amplitude of the observed fringe or *contrast*. Eq. (4) defines a spatio-temporal signal where $\varphi[n]$ are temporal phase shifts and where $\omega x_{\mathrm{PRJ}} = \Phi$ is a spatial phase. The spatial phase Φ cannot be recovered directly from the N acquired frames. Instead, a wrapped phase $\phi \equiv \Phi \pmod{2\pi}$ is recovered from Eq. (4) using

$$\phi = \mathrm{atan2}(Y, X) \quad (5)$$

where

$$\begin{aligned} Y &= -\sum\nolimits_{n=0}^{N-1} I_{\mathrm{CAM}}(x_{\mathrm{CAM}}, y_{\mathrm{CAM}}) \sin\big(\varphi[n]\big) \\ X &= \sum\nolimits_{n=0}^{N-1} I_{\mathrm{CAM}}(x_{\mathrm{CAM}}, y_{\mathrm{CAM}}) \cos\big(\varphi[n]\big) \end{aligned}.$$

The wrapped phase ϕ is then unwrapped to obtain Φ using one of the well known phase unwrapping algorithms [32, 6]. Then for each camera pixel $(x_{\mathrm{CAM}}, y_{\mathrm{CAM}})$ the spatial projector coordinate x_{PRJ} is recovered from the spatial phase Φ using

$$x_{\mathrm{PRJ}} = \Phi/\omega. \quad (6)$$

Finally, the surface profile is reconstructed via triangulation [10].

2.2. Two Projectors

Let us now consider the case of two projectors where both projectors simultaneously project sinusoidal fringes patterns so camera observes an additive combination of two sinusoidal fringes for each of N recorded frames.

Adding the contribution of the second projector to Eq. (4) yields

$$I_{\mathrm{CAM}} = a + b_1 \cos(\omega_1 x_1 + \varphi_1) + b_2 \cos(\omega_2 x_2 + \varphi_2), \quad (7)$$

where b_k, ω_k and φ_k are contrast, spatial frequency, and temporal phase shift of kth projector (spatial coordinates are omitted for clarity). In Eq. (7) the term a contains the overall contribution of ambient illumination and of both projectors,

$$a = I_{\mathrm{AMB}} + \frac{1}{2}hI_1 + \frac{1}{2}hI_2, \quad (8)$$

where I_1 and I_2 replace I_0 of Eq. (2). Let $\phi_1 = \omega_1 x_1$ and $\phi_2 = \omega_2 x_2$ be spatial wrapped phases of the first and the second projector respectively. Then

$$I_{\text{CAM}}[n] = a + b_1 \cos(\phi_1 + \varphi_1[n]) + b_2 \cos(\phi_2 + \varphi_2[n]), \quad (9)$$

which may be decomposed into a sum of five complex exponentials

$$I_{\text{CAM}}[n] = ae^{j0} + \tfrac{1}{2}b_1 e^{j\phi_1} e^{j\varphi_1[n]} + \tfrac{1}{2}b_1 e^{-j\phi_1} e^{-\varphi_1[n]}$$
$$+ \tfrac{1}{2}b_2 e^{j\phi_2} e^{j\varphi_2[n]} + \tfrac{1}{2}b_2 e^{-j\phi_2} e^{-\varphi_2[n]}. \quad (10)$$

Recall a standard notation from digital signal processing [15] where a time-discrete complex exponential with the period N is denoted by

$$W_N^n = \exp(-2\pi j n / N). \quad (11)$$

Specifically, W_N is the Nth root of unity and

$$\langle W_N^{nk_1}, W_N^{nk_2} \rangle = \sum_{n=0}^{N-1} W_N^{-nk_1} W_N^{nk_2}$$
$$= \begin{cases} 0, & k_1 \not\equiv k_2 \ (\text{mod } N) \\ N, & k_1 \equiv k_2 \ (\text{mod } N) \end{cases} \quad (12)$$

holds. We say that time-discrete complex exponentials of period N form an orthogonal basis with N basis vectors $v_k[n] = W_N^{nk}$, where $n = 0, \ldots, N-1$ is time-step and where $k = 0, \ldots, N-1$ is basis vector index.

We propose that each projector uses a different set of temporal phase shifts so

$$\varphi_1[n] = 2\pi n / N \ \text{ and } \ \varphi_2[n] = 4\pi n / N = 2\varphi_1[n]. \quad (13)$$

Eq. (10) may be rewritten using Eqs. (11) and (13) to obtain

$$I_{\text{CAM}}[n] = aW_N^{0 \cdot n} + \tfrac{1}{2}b_1 e^{j\phi_1} W_N^{-n} + \tfrac{1}{2}b_1 e^{-j\phi_1} W_N^{n}$$
$$+ \tfrac{1}{2}b_2 e^{j\phi_2} W_N^{-2n} + \tfrac{1}{2}b_2 e^{-j\phi_2} W_N^{2n}, \quad (14)$$

which is a decomposition of the time-discrete signal $I_{\text{CAM}}[n]$ into a sum of complex exponentials W_N^{nk}. The decomposition of Eq. (14) is recognizable as the discrete Fourier transform in N points of $I_{\text{CAM}}[n]$ [15]. More specifically

$$\hat{I}_{\text{CAM}}[k] = \text{DFT}_N \big[I_{\text{CAM}}[n] \big] = \quad (15)$$
$$= \{ \tfrac{N}{2}b_2 e^{j\phi_2}, \tfrac{N}{2}b_1 e^{j\phi_1}, \underline{Na}, \tfrac{N}{2}b_1 e^{-j\phi_1}, \tfrac{N}{2}b_2 e^{-j\phi_2} \}.$$

We say $\hat{I}_{\text{CAM}}[k]$ is a five component discrete spectrum of $I_{\text{CAM}}[n]$. In Eq. (15) the DC spectral component models the ambient illumination and mean projector intensities. Two additional spectral components are required to model each

projector, $k = \pm 1$ for the first projector and $k = \pm 2$ for the second. If the number of temporal phase shifts N satisfies $N \geq 2 \cdot 2 + 1 = 5$ then all complex exponentials in Eq. (14) are orthogonal and the decomposition of N observed frames into contributions of each projector is possible.

To recover the kth wrapped phase ϕ_k the fast Fourier transform [4] may be used to pixel-wise decompose N acquired frames and compute the spectrum (15). The wrapped phase ϕ_k is the argument of the spectrum at the index k:

$$\phi_k = -\text{Arg}(\hat{I}_{\text{CAM}}[k]) = -\text{Arg}(\tfrac{N}{2}b_k e^{-j\phi_k}). \quad (16)$$

Similarly, the contrast b_k may be computed from the absolute value of the spectrum at the index k:

$$b_k = \tfrac{2}{N} \big| \hat{I}_{\text{CAM}}[k] \big|. \quad (17)$$

Although the contrast b_k is not required for phase recovery it is used to determine if a particular camera pixel is illuminated by the kth projector. The value of contrast is compared to some threshold T and pixels for which

$$b_k > T \quad (18)$$

holds are considered illuminated by the k-th projector. The threshold T is best set as a percentage of $\frac{1}{2}I_k$, e.g. setting T to 10% of $\frac{1}{2}I_k$ requires that channel loss h is no lower than 0.1. Once wrapped phases ϕ_1 and ϕ_2 are computed the surface profile may be reconstructed for each projector-camera pair as was described in Section 2.1.

2.3. Arbitrary Number of Projectors

Let us now consider the arbitrary number of projectors where all projectors project their sinusoidal fringes simultaneously. The camera now observes an additive combination of all fringes in each of N acquired frames.

Let $P \geq 1$ be the number of projectors. Then Eq. (9) generalizes to

$$I_{\text{CAM}}[n] = a + \sum_{k=1}^{P} b_k \cos(\phi_k + \varphi_k[n]). \quad (19)$$

Instead of a single sinusoidal fringe we are observing a sum of P fringes. We propose to select the P temporal phase shifts $\varphi_k[n]$ so

$$\varphi_k[n] = 2\pi kn / N, \quad k = 1, \ldots, P. \quad (20)$$

Using the selected temporal phase shifts Eq. (19) transforms to

$$I_{\text{CAM}}[n] = a + \sum_{k=1}^{P} \tfrac{1}{2}b_k \big(e^{j\phi_k} W_N^{-kn} + e^{-j\phi_k} W_N^{kn} \big), \quad (21)$$

which is a discrete Fourier transform decomposition of the signal $I_{\text{CAM}}[n]$ in $2P + 1$ points and is a generalization of

Eq. (14). In the proposed decomposition the ambient illumination and the combined mean projector intensity of all P projectors are modeled by the term a which has the basis vector $W_N^{0 \cdot n}$. The sinusoidal fringe of the kth projector is modeled by a single summand of the sum in Eq. (21) which uses two basis vectors $W_N^{-k \cdot n}$ and $W_N^{k \cdot n}$. As each projector uses a different phase-shift step k the decomposition of Eq. (21) is unambiguous if

$$N \geq 2P + 1. \tag{22}$$

Wrapped phases and contrast may then be recovered using Eqs. (16) and (17). Applying a phase unwrapping algorithm [32, 6] recovers coordinates x_{PRJ} which together with known x_{CAM} and y_{CAM} enable surface reconstruction via triangulation [10].

To summarize, the proposed method for multi-projector multi-camera FPP scanning is comprised of the following steps:

1. For each of P projectors generate a set of $N \geq 2P+1$ fringe patterns using Eq. (2) where the temporal phase shift of kth projector is given by Eq. (20).

2. Set P projectors to simultaneously project fringes so each camera observes N frames containing an additive combination of projected fringes.

3. For each camera decode the set of N observed frames as follows:

   (a) Decompose in time the set of N frames using the fast Fourier transform in N points.

   (b) Determine the area illuminated by the kth projector using Eq. (18).

   (c) Recover the wrapped phase ϕ_k for the area illuminated by the kth projector using Eq. (16).

   (d) Unwrap the wrapped phase ϕ_k using any of the algorithms from [32, 6] to obtain Φ_k.

   (e) Recover the projector coordinate $x_{\mathrm{PRJ},k}$ of kth projector from Φ_k using Eq. (6).

4. Triangulate object's surface using all collected camera and projector coordinate pairs.

3. Comparison to Sequential Employment

The simplest data acquisition strategy for multi-projector multi-camera SL system which avoids inter-projector interference is to use each projector in turn [26, 5], a so-called *sequential* projector employment. The proposed method uses projectors *simultaneously* which allows the reduction in the total number of *acquisitions*, where an *acquisition* means a simultaneous frame capture on all cameras.
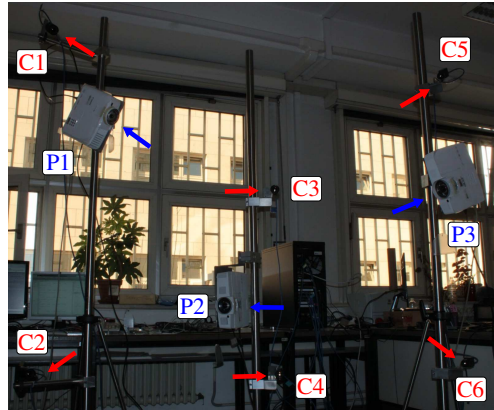

Figure 1. Multi-projector multi-camera structured light 3D scanner comprised of three projectors and six cameras mounted on three vertical poles.
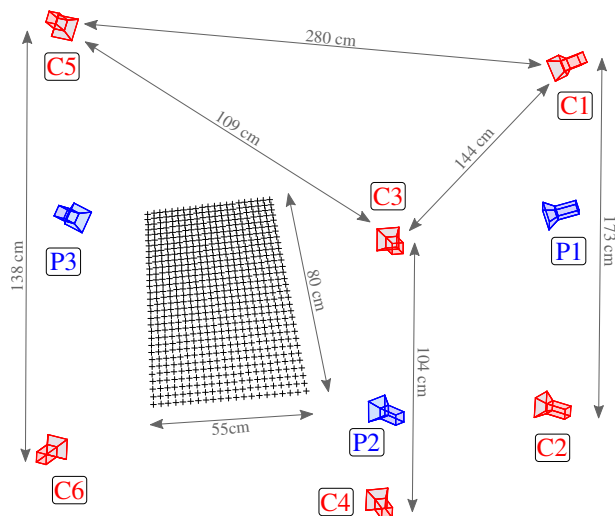

Figure 2. Spatial arrangement for 3D scanner. One projector and one camera-pair are mounted on the same vertical pole as follows: C1-P1-C2 on the first pole, C3-P2-C4 on the second, and C5-P3-C6 on the third. Points for one position of a planar calibration board are shown as black crosses.

For a single projector the minimum number of sinusoidal fringes to project is 3 [2, 3], so for P projectors employed sequentially the minimum number of acquisitions is $3P$. The proposed method reduces $3P$ to $2P + 1$, which is a clear advantage. Furthermore, in practice the number of phase shifts is never the minimum 3 due to noise sensitivity; common choices are 7 or more shifts [3]. For the proposed method all acquired frames contain data of more (all) projectors, therefore for three or more projectors we achieve 7 or more shifts for each projector as $2P + 1 > 7$.

A disadvantage of the proposed method compared to sequential employment is that simultaneous employment makes camera's dynamic range shared between projectors. In an ideal one-projector setup a whole camera's dynamic
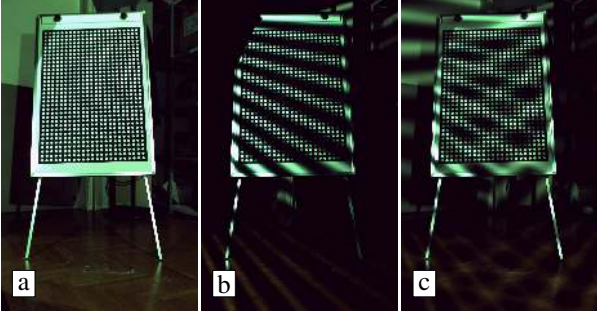
Figure 4. A planar calibration board used for quantitative analysis as seen by C4: (a) board under white illumination; (b) board under illumination by P3 using ω_2; and (c) board under illumination by all three projectors simultaneously. Note the difference between the pure fringe in (b) and the multi-projector interference pattern in (c).

	P1	P2	P3
C1	0.15 ± 3.26	0.10 ± 0.08	0.12 ± 0.12
C2	0.15 ± 2.73	0.09 ± 0.08	0.11 ± 0.10
C3	0.16 ± 3.72	0.13 ± 0.12	0.17 ± 4.23
C4	0.21 ± 5.52	0.21 ± 5.31	0.15 ± 4.20
C5	0.12 ± 0.11	0.11 ± 0.10	0.15 ± 3.68
C6	0.18 ± 4.08	0.13 ± 0.12	0.15 ± 3.05

Table 2. Absolute mean error of recovered projector coordinate x_{PRJ} expressed in projector pixels and its standard deviation for a planar calibration board shown in Fig. 4. Note the average error is in subpixel range at about $0.14\,\mathrm{px}$.

range D is allocated to that projector. However, in multi-projector setup each camera observes the sum which reduces the maximal dynamic range allocated to one projector to D/P. This reduction increases measurement noise and may affect wrapped phase estimation. Fortunately, the loss of resolution in amplitude due to sharing of the dynamic range may be compensated by using a better camera or by increasing the temporal resolution by using more phase shifts.

In practice the loss of resolution in amplitude has a firm limit which is determined by the number of projectors with overlapping FOVs. That limit is normally less than the total number of projectors used, e.g. to scan a complete human body P projectors are placed to surround the human which in practice limits the overlap to about 2 or 3 projectors instead of P.

In the context of multiplexed-illumination as proposed by Schechner et al. [23] a multi-projector SL scanner operates in saturation-limited range: camera exposure must be fixed to match the common refresh rate of all projectors, therefore only lens iris is used to avoid oversaturation. Then, comparing sequential acquisition using M shifts for each of P spatial frequencies with the proposed simultaneous acquisition using $N = 2P + 1$ shifts yields an SNR gain of N/M in the signal amplitude (contrast) b and of $(N \cdot B_1^2)/(M \cdot B_2^2)$ in the signal phase φ [14, 12], where $B_1 = D/P$ and $B_2 = D$ are fringe modulations. In practice using an 8-bit camera is sufficient to separate patterns of at least three overlapping projectors.

4. Results and Discussion

To demonstrate the applicability of the proposed method we have built a SL scanner comprised of three projectors and six cameras shown in Fig. 1. Of three projectors one is Canon LV-WX310ST (P1) and two are Acer S1383WHne (P2,P3). All projectors are operated at their

native resolution of 1280×800. All six cameras are Point-Grey's Grasshopper3 GS3-U3-23S6C-C; four cameras are fitted with Fujinon HF12.5SA-1 lenses (C1,C2,C3,C4) and two with Kowa LM8JCM lenses (C5,C6). The scanner is synchronized in software and acquires images at 20 FPS. The system was calibrated using a planar calibration board (Fig. 4) and the method of [17, 10]. The spatial arrangement of projectors and cameras is shown in Fig. 2; note that Fig. 1 is a view toward the scanner and Fig. 2 is a view toward the object. Such an arrangement was deliberately chosen to maximize projector overlap and to better demonstrate the proposed method; there is no camera-projector pair for which the common field-of-view is empty. In real-world applications and especially in human body scanning a setup where projectors and cameras surround the object would normally be used.

We have selected a multiple-phase shifting (MPS) unwrapping strategy [18] with three spatial frequencies $\omega_0 = 2\pi\frac{13}{W}$, $\omega_1 = 2\pi\frac{17}{W}$, and $\omega_2 = 2\pi\frac{21}{W}$, where $W = 1280\,\mathrm{px}$ is projector width. Fringes are projected in a round-robin fashion: first P1 projects ω_0, P2 ω_1, and P3 ω_2 using N phase-shifts each; then pth projector switches its spatial frequency from ω_m to $\omega_{m+1 \,(\mathrm{mod}\,3)}$ etc. The number of phase shifts was set to $N = 12$. The phase steps were chosen to be 1, 3, and 5 so P1 used $\varphi_1[n] = \frac{1}{6}\pi n$, P2 $\varphi_2[n] = \frac{1}{2}\pi$, and P3 $\varphi_3[n] = \frac{5}{6}\pi n$. We have performed several experiments using these parameters: (i) a quantitative comparison of wrapped phases; (ii) a quantitative comparison of recovered projector coordinate; and (iii) a 3D reconstruction of a person. Concerning the operating scanner frame rate of 20 FPS, the number of 12 phase shifts, the number of 3 frequencies, and the number of 3 projectors involved, the acquisition times for sequential and simultaneous scanning are approximately 5.5 and 1.8 seconds respectively.

We quantitatively compare wrapped phases and recovered projector coordinate to the classical MPS strategy which is taken as the ground truth. Recorded object is a
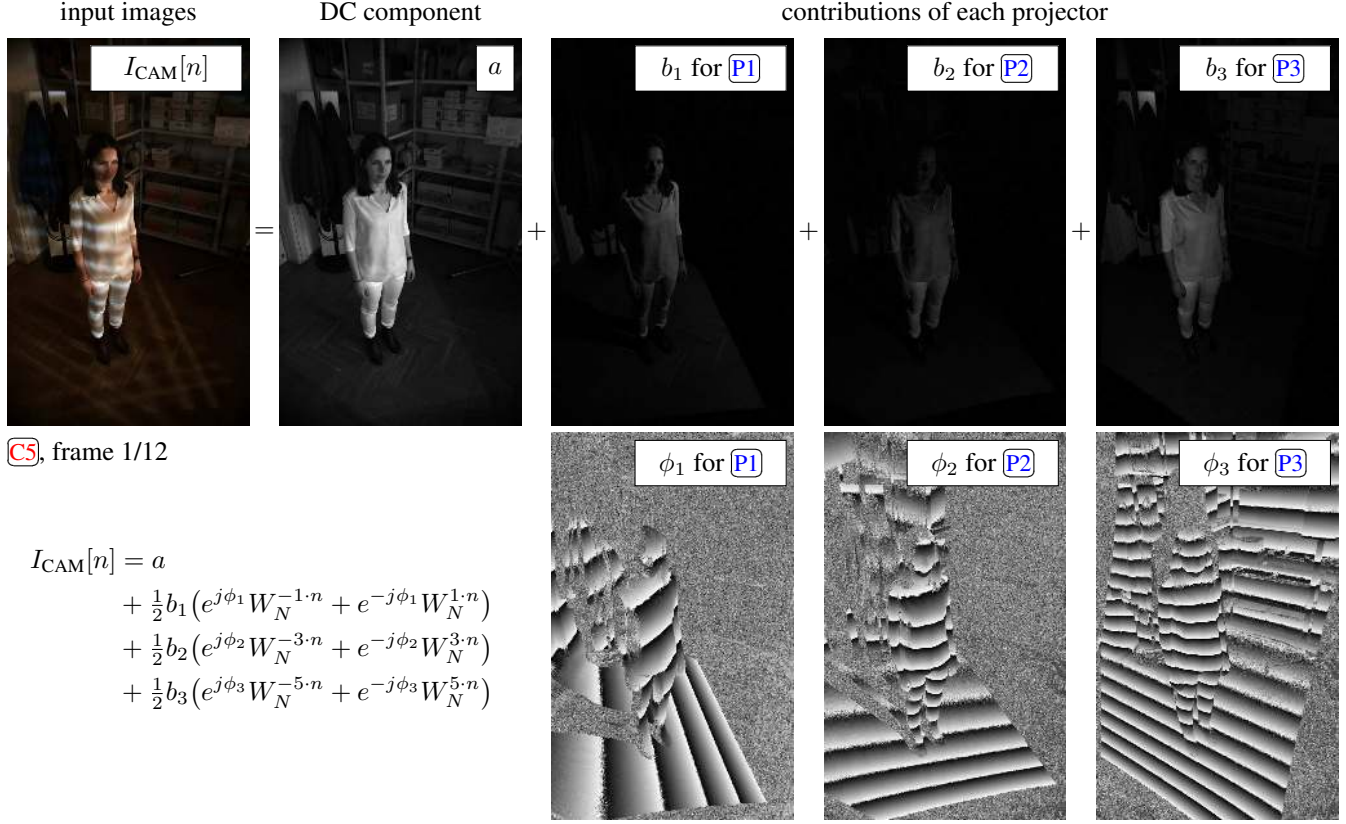
input images | DC component | contributions of each projector

$I_{\mathrm{CAM}}[n]$

a

b_1 for P1

b_2 for P2

b_3 for P3

C5, frame 1/12

ϕ_1 for P1

ϕ_2 for P2

ϕ_3 for P3

$$
\begin{aligned}
I_{\mathrm{CAM}}[n] = \; & a \\
& + \tfrac{1}{2}b_1\big(e^{j\phi_1}W_N^{-1\cdot n} + e^{-j\phi_1}W_N^{1\cdot n}\big) \\
& + \tfrac{1}{2}b_2\big(e^{j\phi_2}W_N^{-3\cdot n} + e^{-j\phi_2}W_N^{3\cdot n}\big) \\
& + \tfrac{1}{2}b_3\big(e^{j\phi_3}W_N^{-5\cdot n} + e^{-j\phi_3}W_N^{5\cdot n}\big)
\end{aligned}
$$

Figure 3. Spectral decomposition for C5. Twelve input frames are decomposed using the proposed method to obtain contributions of each individual projector. Note that ϕ_1 has spatial frequency $\omega_0 = 2\pi\frac{13}{W}$, ϕ_2 has $\omega_1 = 2\pi\frac{17}{W}$, and ϕ_3 has $\omega_2 = 2\pi\frac{21}{W}$.

stationary calibration board (Fig. 4) which was first imaged using sequential employment (classical MPS) and then using the proposed method (simultaneous employment). Wrapped phases are compared using the absolute circular distance $d_{\mathrm{circular}}(\cdot,\cdot)$ as the error metric:

$$
d_{\mathrm{circular}}(\phi, \phi_{\mathrm{MPS}}) = \big| \mathrm{Arg}(e^{i\phi}/e^{i\phi_{\mathrm{MPS}}})\big|, \qquad (23)
$$

where ϕ is the wrapped phase obtained using Eq. (16) and ϕ_{MPS} is the ground truth. The error metric was computed for illuminated pixels only using the threshold T of 5%. Table 1 lists errors for all $3 \cdot 3 \cdot 6 = 54$ (number of spatial frequencies used times number of projectors times number of cameras) wrapped phases. On average the wrapped phase error is $0.0168\,\mathrm{rad} = 0.96°$. The absolute error in the recovered projector coordinate, $|x_{\mathrm{PRJ}} - x_{\mathrm{PRJ,MPS}}|$, is listed in Table 2 for all $3 \cdot 6 = 18$ camera-projector combinations. On average the projector coordinate error is $0.14\,\mathrm{px}$. Note that the distribution of errors is not Gaussian and that quantitative results are presented using non-filtered data. Overall, almost all ($> 95\%$) points have error below the twice the mean and only a small number of outliers affects the deviation for some views. These quantitative results clearly indicate the applicability of the proposed method.

For a qualitative evaluation of the proposed scanner we

have recorded a female model in an office during the day under normal ambient illumination. An example of spectral decomposition of the first 12 input frames for C5 is shown in Fig. 3. Note the following: (1) the DC component a contains both ambient and average illumination of all projectors; (2) the contrast b_k indicates which areas are well illuminated by kth projector; and (3) the wrapped phase ϕ_k is recovered even for poorly illuminated areas as ϕ_k is mostly independent of b_k. The spectral decomposition is then applied to all 36 input frames to obtain three wrapped phases for each of six cameras. Wrapped phases may then be unwrapped using the method of [18]. An example of nine wrapped phases and of recovered projector coordinates is shown in Fig. 5. In Figs. 3 and 5 processing results are shown for all pixels, i.e. even pixels which are not illuminated according to Eq. (18) were processed.

Once projector coordinates are known for each camera a 3D point cloud is obtained via triangulation [10]. Recovered 3D surface points may be textured using the value of a as the gray-level intensity. Furthermore, if cameras are recording in color then the DC spectral coefficient a may be computed for each color channel separately. This yields a full-color texture with the sinusoidal fringe removed: there is no need to acquire an additional frame with all projec-

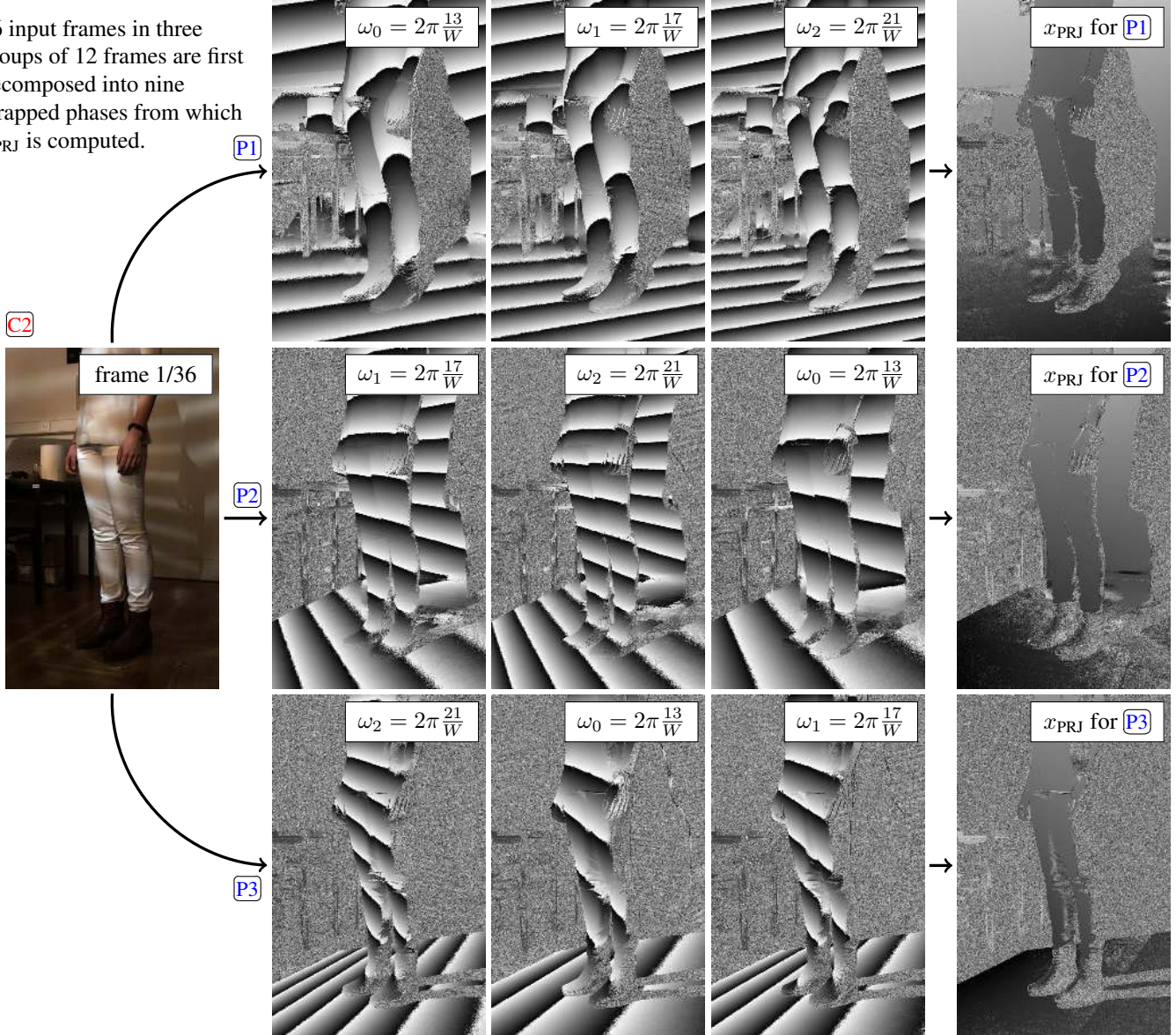36 input frames in three groups of 12 frames are first decomposed into nine wrapped phases from which x_{PRJ} is computed.

C2

P1

P2

P3

frame 1/36

$\omega_0 = 2\pi\frac{13}{W}$ $\omega_1 = 2\pi\frac{17}{W}$ $\omega_2 = 2\pi\frac{21}{W}$ x_{PRJ} for P1

$\omega_1 = 2\pi\frac{17}{W}$ $\omega_2 = 2\pi\frac{21}{W}$ $\omega_0 = 2\pi\frac{13}{W}$ x_{PRJ} for P2

$\omega_2 = 2\pi\frac{21}{W}$ $\omega_0 = 2\pi\frac{13}{W}$ $\omega_1 = 2\pi\frac{17}{W}$ x_{PRJ} for P3

Figure 5. Recovered wrapped phases and projector coordinates for C2. Note different shadows in the projector coordinate x_{PRJ} for three projectors.

	P1			P2			P3		
	ω_0	ω_1	ω_2	ω_0	ω_1	ω_2	ω_0	ω_1	ω_2
C1	0.91 ± 0.81	1.16 ± 1.75	0.91 ± 0.75	0.95 ± 0.74	0.75 ± 0.58	0.75 ± 0.60	0.76 ± 0.62	0.76 ± 0.62	1.07 ± 1.14
C2	0.95 ± 0.89	1.20 ± 1.85	0.94 ± 0.77	0.92 ± 0.73	0.58 ± 0.43	0.77 ± 0.56	0.77 ± 0.63	0.77 ± 0.62	0.99 ± 0.94
C3	1.12 ± 4.51	0.86 ± 0.70	0.89 ± 1.71	0.96 ± 0.93	0.96 ± 0.88	1.25 ± 1.23	0.86 ± 0.75	1.01 ± 1.82	0.88 ± 0.78
C4	1.41 ± 9.32	0.83 ± 0.93	0.86 ± 3.53	1.26 ± 4.91	1.06 ± 1.00	2.02 ± 11.24	0.84 ± 0.71	0.96 ± 0.86	0.86 ± 0.74
C5	0.79 ± 0.66	0.78 ± 0.65	1.15 ± 1.35	0.86 ± 0.80	1.02 ± 1.01	0.85 ± 0.80	1.04 ± 3.15	0.89 ± 0.73	0.89 ± 0.77
C6	0.82 ± 0.97	0.79 ± 0.72	1.28 ± 3.01	1.00 ± 0.89	1.32 ± 1.19	1.00 ± 0.87	1.01 ± 1.30	0.87 ± 0.73	0.87 ± 0.75

Table 1. Absolute wrapped phase error of recovered wrapped phases ϕ in degrees and its standard deviation for a planar calibration board shown in Fig. 4.
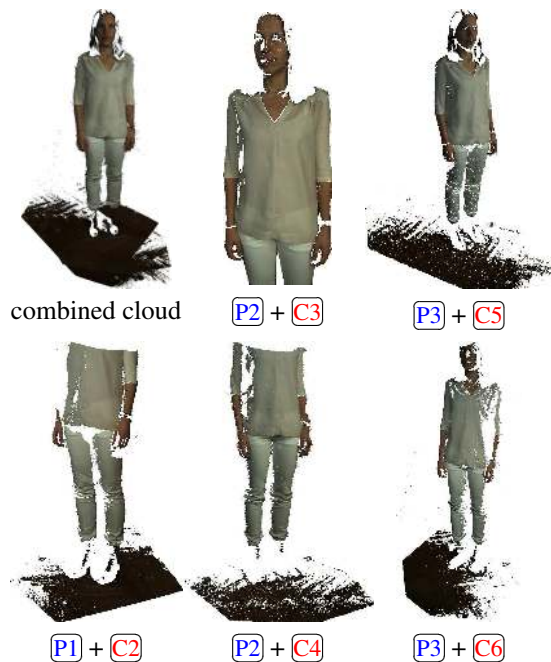
Figure 6. Textured point clouds for a recorded female model. Holes in the reconstructed point clouds originated from the limited camera dynamic range, required to capture both very dark and very bright surface parts.

tors turned off (or projecting all-white pattern). A textured point clouds for a female model are shown in Fig. 6. For this reconstruction we have used the threshold T of 10% which effectively removes dark areas such as model's hair and boots together with parts of a hardwood floor. Note that except for selection of illuminated points no additional filtering or smoothing was performed on the data shown in Fig. 6. We also point out that fitting a plane to the 3D reconstructed planar object have shown essentially the same result both for sequential and simultaneous approach (not shown due to the space limitation).

The proposed method uses sinusoidal fringes which are robust to projector and camera blur: the phase is unaffected by blurring due to spatial symmetry of the blurring OTF [13]. This is a highly desirable property and is a clear advantage of the proposed multi-projector FPP approach over non-FPP multi-projector approaches such as [20, 19, 30].

The proposed method opens an exciting possibility of combining FPP and photometric stereo [28] when many projectors are used. Consider three images showing the recovered contrast coefficients b_k which are shown in Fig. 3: the viewing direction is constant while the direction of incident illumination depends on the projector. If sufficient number of viewing directions is known surface orientation may be recovered from the contrast coefficients b_k.

5. Conclusion

We have proposed a method for efficient separation between projected sinusoidal fringe patterns in fringe projection profilometry which is based on a specific choice of temporal phase shifts.

We have shown that for a system of P projectors a selection of temporal phase shifts exists which enables decomposition of the projected fringes in terms of the basis vectors of the discrete Fourier transform in $2P + 1$ or more points. Such decomposition in turn enables efficient separation between projected sinusoidal fringe patterns.

The proposed method does not impose a limit on the number of projectors nor on their placement. This in turn enables construction of large FPP systems comprised of many projectors and cameras which may be particularly useful in human body scanning.

Acknowledgment

References

[1] J. Batlle, E. Mouaddib, and J. Salvi. Recent progress in coded structured light as a technique to solve the correspondence problem: a survey. *Pattern Recognition*, 31(7):963–982, 1998. 1

[2] K. Creath. V phase-measurement interferometry techniques. volume 26 of *Progress in Optics*, pages 349–393. Elsevier, 1988. 2, 4

[3] P. de Groot. Derivation of algorithms for phase-shifting interferometry using the concept of a data-sampling window. *Appl. Opt.*, 34(22):4723–4730, Aug 1995. 4

[4] M. Frigo and S. G. Johnson. FFTW: an adaptive software architecture for the FFT. In *Acoustics, Speech and Signal Processing, 1998. Proceedings of the 1998 IEEE International Conference on*, volume 3, pages 1381–1384 vol.3, May 1998. 3

[5] R. R. Garcia and A. Zakhor. Markerless motion capture with multi-view structured light. *Electronic Imaging*, 2016(21):3DIPM–050.1–3DIPM–050.7, 2016. 1, 4

[6] D. C. Ghiglia and M. D. Pritt. *Two-Dimensional Phase Unwrapping: Theory, Algorithms, and Software*. Wiley, May 1998. 2, 4

[7] S. S. Gorthi and P. Rastogi. Fringe projection techniques: Whither we are? *Optics and Lasers in Engineering*, 48(2):133–140, 2010. 1

[8] J. Gu, T. Kobayashi, M. Gupta, and S. K. Nayar. Multiplexed illumination for scene recovery in the presence of global illumination. In *2011 International Conference on Computer Vision*, pages 691–698, Nov 2011. 2

[9] M. Gupta and S. K. Nayar. Micro phase shifting. In *2012 IEEE Conference on Computer Vision and Pattern Recognition*, pages 813–820, June 2012. 2

[10] R. Hartley and A. Zisserman. *Multiple view geometry in computer vision*. Cambridge university press, 2003. 2, 4, 5, 6

[11] J. M. Huntley and H. O. Saldner. Shape measurement by temporal phase unwrapping: comparison of unwrapping algorithms. *Measurement Science and Technology*, 8(9):986, 1997. 2

[12] B. Kamgar-Parsi and B. Kamgar-Parsi. Evaluation of quantization error in computer vision. *IEEE Transactions on Pattern Analysis and Machine Intelligence*, 11(9):929–940, Sep 1989. 5

[13] B. Li, N. Karpinsky, and S. Zhang. Novel calibration method for structured-light system with an out-of-focus projector. *Appl. Opt.*, 53(16):3415–3426, Jun 2014. 8

[14] J. Li, L. G. Hassebrook, and C. Guan. Optimized two-frequency phase-measuring-profilometry light-sensor temporal-noise sensitivity. *J. Opt. Soc. Am. A*, 20(1):106–115, Jan 2003. 5

[15] S. K. Mitra. *Digital Signal Processing: A Computer-Based Approach*. McGraw-Hill Companies, 3 edition, Jan. 2005. 3

[16] D. Moreno, K. Son, and G. Taubin. Embedded phase shifting: Robust phase shifting with embedded signals. In *2015 IEEE Conference on Computer Vision and Pattern Recognition (CVPR)*, pages 2301–2309, June 2015. 2

[17] D. Moreno and G. Taubin. Simple, accurate, and robust projector-camera calibration. In *2012 Second International Conference on 3D Imaging, Modeling, Processing, Visualization Transmission*, pages 464–471, Oct 2012. 5

[18] T. Petković, T. Pribanić, and M. Đonlić. Temporal phase unwrapping using orthographic projection. *Optics and Lasers in Engineering*, 90:34–47, 2017. 5, 6

[19] R. Sagawa, R. Furukawa, and H. Kawasaki. Dense 3d reconstruction from high frame-rate video using a static grid pattern. *IEEE Transactions on Pattern Analysis and Machine Intelligence*, 36(9):1733–1747, Sept 2014. 1, 8

[20] R. Sagawa, Y. Ota, Y. Yagi, R. Furukawa, N. Asada, and H. Kawasaki. Dense 3d reconstruction method using a single pattern for fast moving object. In *2009 IEEE 12th International Conference on Computer Vision*, pages 1779–1786, Sept 2009. 1, 8

[21] J. Salvi, S. Fernandez, T. Pribanić , and X. Lladó. A state of the art in structured light patterns for surface profilometry. *Pattern Recognition*, 43(8):2666–2680, 2010. 1

[22] J. Salvi, J. Pagès, and J. Batlle. Pattern codification strategies in structured light systems. *Pattern Recognition*, 37(4):827–849, 2004. 1

[23] Y. Y. Schechner, S. K. Nayar, and P. N. Belhumeur. Multiplexing for optimal lighting. *IEEE Transactions on Pattern Analysis and Machine Intelligence*, 29(8):1339–1354, Aug 2007. 5

[24] M. Servin, G. Garnica, J. C. Estrada, and A. Quiroga. Coherent digital demodulation of single-camera n-projections for 3d-object shape measurement: Co-phased profilometry. *Opt. Express*, 21(21):24873–24878, Oct 2013. 1

[25] M. Servin, M. Padilla, G. Garnica, and A. Gonzalez. Profilometry of three-dimensional discontinuous solids by combining two-steps temporal phase unwrapping, co-phased pro-

[26] W.-H. Su, C.-Y. Kuo, C.-C. Wang, and C.-F. Tu. Projected fringe profilometry with multiple measurements to form an entire shape. *Opt. Express*, 16(6):4069–4077, Mar 2008. 1, 4

[27] L. X. Tang, J. Chen, and H. L. Chen. A novel structured light pattern for one-shot shape acquisition. In *Frontiers of Manufacturing Science and Measuring Technology III*, volume 401 of *Applied Mechanics and Materials*, pages 1191–1194. Trans Tech Publications, 12 2013. 1

[28] R. J. Woodham. Photometric method for determining surface orientation from multiple images. *Optical Engineering*, 19(1):191139–191139–, 1980. 8

[29] S. Woolford and I. S. Burnett. Toward a one shot multi-projector profilometry system for full field of view object measurement. In *2014 IEEE International Conference on Acoustics, Speech and Signal Processing (ICASSP)*, pages 569–573, May 2014. 1, 2

[30] Z. Yan, L. Yu, Y. Yang, and Q. Liu. Beyond the interference problem: hierarchical patterns for multiple-projector structured light system. *Appl. Opt.*, 53(17):3621–3632, Jun 2014. 2, 8

[31] Z. Zhang. Review of single-shot 3d shape measurement by phase calculation-based fringe projection techniques. *Optics and Lasers in Engineering*, 50(8):1097–1106, 2012. 1, 2

[32] C. Zuo, L. Huang, M. Zhang, Q. Chen, and A. Asundi. Temporal phase unwrapping algorithms for fringe projection profilometry: A comparative review. *Optics and Lasers in Engineering*, 85:84–103, 2016. 2, 4

filometry and phase-shifting interferometry. *Optics and Lasers in Engineering*, 87:75–82, 2016. 1